Supplementary information for

Formation of chloride deposits on Early Mars under acidic and reducing crustal conditions

David C Fernández-Remolar[1,2*], Wladyslaw Altermann[3], David Gomez-Ortiz[4], Brian Hynek[5,6], Matthew R.M. Izawa[7], Ernst Hauber[8], Solmaz Adeli[8], Ricardo Amils[9], Ting Huang[10,11], Angelo Pio Rossi[12], Laetitia Le Deit[13]

[1]National Space Science and Technology Center, United Arab Emirates University, Al Ain, UAE. [2]Univ Grenoble Alpes, CEA, CNRS, IBS, Metalloproteins Unit, F-38000 Grenoble, France. [3]Dept. of Geology, University of Johannesburg, South Africa. [4]ESCET-Área de Geología, Universidad Rey Juan Carlos, 28933 Móstoles, Madrid, Spain. [5]Laboratory for Atmospheric and Space Physics, University of Colorado–Boulder, 3665 Discovery Drive, Boulder, Colorado 80303, USA. [6]Department of Geological Sciences, University of Colorado–Boulder, UCB399, Boulder, Colorado 80309, USA. [7]Institute for Planetary Materials, Okayama University, Misasa, Tottori, 682-0193, Japan. [8]Institute of Planetary Research, German Aerospace Center (DLR), Berlin, Germany. [9]Planetology and Habitability Department, Center of Astrobiology (INTA-CSIC), Torrejón de Ardoz, 28850 Madrid, Spain. [10]State Key Laboratory of Lunar and Planetary Sciences, Macau University of Science and Technology, Macau 999078, PR China. [11]CNSA Macau Center for Space Exploration and Science, Macau 999078, PR China. [12]Jacobs University Bremen, Campus Ring 1, 28759 Bremen, Germany. [13]Laboratoire de Planétologie et Géodynamique, LPG-Nantes, UMR CNRS, Université de Nantes, Nantes, France.

* Correspondence should be addressed to D.C.F.-R. (email: david.remolar@uaeu.ac.ae).

.

This PDF file includes:

Description of the hydrothermal alteration reactions

Figs. S1 to S10

Tables S1 to S4

Description of the hydrothermal alteration reactions

The main hydrothermal equation describing the acidification process as the following:

Anorthite + Fayalite + Forsterite + Diopside + Albite + 21·H_2O + 4.91·Al^{3+} + 3.91·Mg^{2+} + 2·Fe^{2+} → 1.3·Clinoclore-14Å + 2·Chamosite + 0.75·Montmorilonite-Ca + 0.76·Ca^{2+} + Na^{+} + 21.83·H^{+}, where the end-members anorthite and albite represent the plagioclase feldspar solid solution, and similarly fayalite and forsterite end-members represent the olivine solid solution.

It results from the combination of different reactions that describe acidification under hydrothermal activity discussed by Seyfried (1987). Such a process is driven by cation mesomatism that promotes acidification through a secondary hydrolysis reaction (e.g. Mg^{2+} +2·H_2O → $Mg(OH)_2$ + 2·H^{+}) operating in a basaltic crust. Thus, the metasomatism reaction can run in the Martian crust that has a similar composition to the oceanic crust, if the structural, hydrological and thermal settings are right. The presence of some cations like Mg^{2+} in the hydrothermal solution has a dominating effect on pH even at temperatures as low as 70 ˚C (Seyfreid, 1987).

The metasomatic hydrothermal reactions were obtained from a combination of the simple reactions **A** to **E** that are listed below, and which have been described by Seyfried (1987) occurring on minerals like anorthite, but affecting olivine as well. Such reactions are included in the thermodynamic database thermo.com V8.R6+ that was used within Geochemist Workbench 11 to perform the geochemical modelling of the salt formation. Note that the reactions involving anorthite and albite, and those involving fayalite and forsterite, can be regarded as acting upon those end-member molecules in the solid solutions of plagioclase feldspar and olivine respectively.

(A) 3·Anorthite ($CaAl_2Si_2O_8$) + 12·H_2O + 10·Mg^{2+} → 8·H^{+} + 3·Ca^{2+} + 2·Al^{3+} + 2·Clinochlore-14 Å ($Mg_5Al_2Si_3O_{10}(OH)_8$)

Equilibrium equation: log $K_{300^{\circ}C}$ (~ -6.9) = 2.667 log a[H+] + log a[Ca++] + .6667 log a[Al+++] - 3.333 log a[Mg++]

(B) 3·Forsterite (Mg_2SiO_4) ***+ 6·H_2O + 2·Al^{3+} → 4·H^+ + Clinochlore-14 Å ($Mg_5Al_2Si_3O_{10}(OH)_8$) + Mg^{2+}***

Equilibrium equation: log $K_{300^\circ C}$ (~ 5.608) = 1.333 log a[H+] + .3333 log a[Mg++] - .6667 log a[Al+++]

(C) 3·Fayalite (Fe_2SiO_4) + 6·H_2O + 2·Al^{3+} + 5·Mg^{2+} → 4·H^+ + Clinochlore-14 Å ($Mg_5Al_2Si_3O_{10}(OH)_8$) + 6·Fe^{2+}

Equilibrium equation: Log $K_{300^\circ C}$ (~ 0.9371) = 1.333 log a[H+] + 2 log a[Fe++] - .6667 log a[Al+++] - 1.667 log a[Mg++]

(D) Diopside ($MgCaSi_2O_6$) + 12·H_2O + 4·Al^{3+} + 4·Fe^{2+} → 16·H^+ + 2·Chamosite-7 Å ($Fe_2Al_2SiO_5(OH)_4$) + Mg^{2+} + Ca^{2+}

Equilibrium equation: log $K_{300^\circ C}$ (8.652) = 16 log a[H+] + log a[Mg++] + log a[Ca++] - 4 log a[Al+++] - 4 log a[Fe++]

(E) 3·Albite ($NaAlSi_3O_8$) + 0.7575·Al^{3+} + 3·H_2O + 0.725·Mg^{2+} + 0.3712·Ca^{2+} → 1.5·H^+ + 2.25·Montmor-Ca ($Ca_{0.16}Mg_{0.33}Al_{0.67}Si_4O_{10}(OH)_2$) + 3·$Na^+$

Equilibrium equation: log $K_{300^\circ C}$ (~ 4.815) = .5 log a[H+] - .2525 log a[Al+++] + log a[Na+] - .2475 log a[Mg++] - .1238 log a[Ca++]

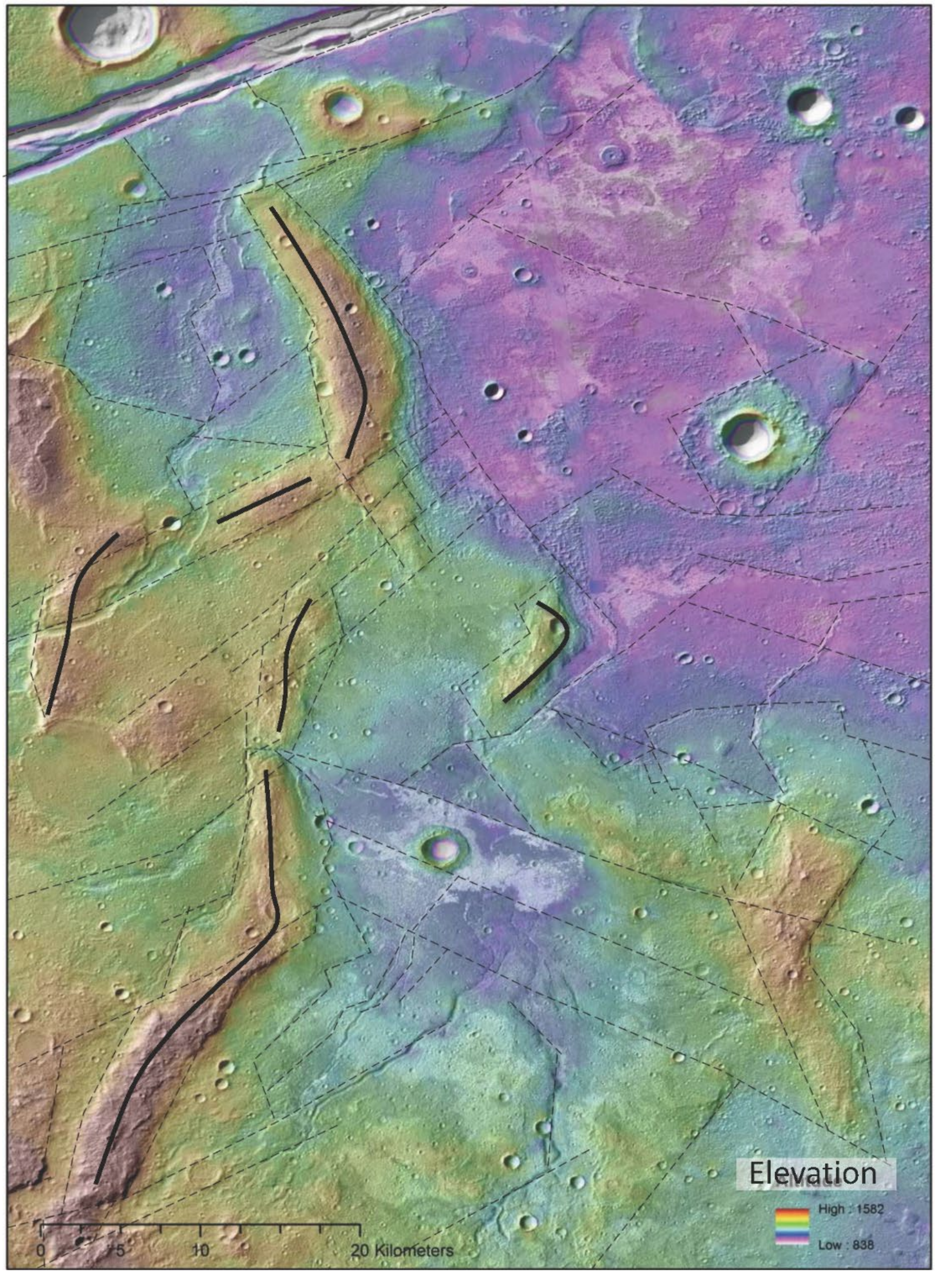

Fig. S1. Structural map of the Noachian basement with chloride deposits in the Sirenum Fossae area, which is shown in Fig. 1. It shows a mixed system of two sets of ENE-WSW and ESE-WNW faults (traced as thin dashed lines), which are crosscutting the N-S normal faults outlined by thick black lines. The main N-S ridges are defined by topographic relief that has configured the emergence and the compartmentalisation of small saline basins. In addition, the morphology of the sedimentary and fluvial structures is strongly constrained by the directions of the minor faults.

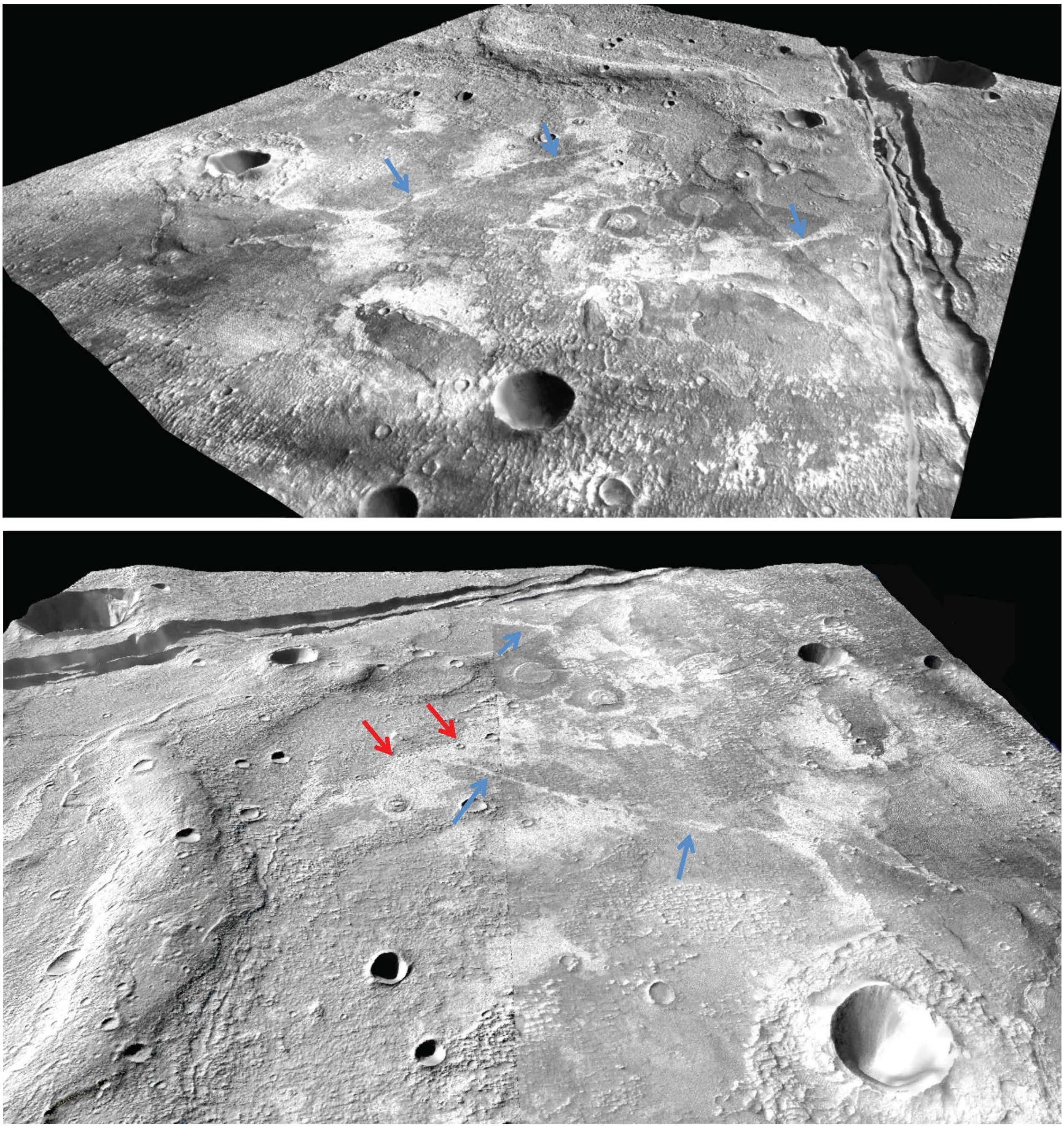

Fig. S2. Two different perspective views of the northern area with salt outcrops described in this work. Blue arrows mark structural lineaments that are covered with salts observed in Fig. 2. In some cases, those salt bodies show straight and rectilinear boundaries (red arrows) suggesting that they are constrained and delimited by faults. As is evident, the linear morphologies of the ridges delineate the main relief that confines the morphologies of the saline basins.

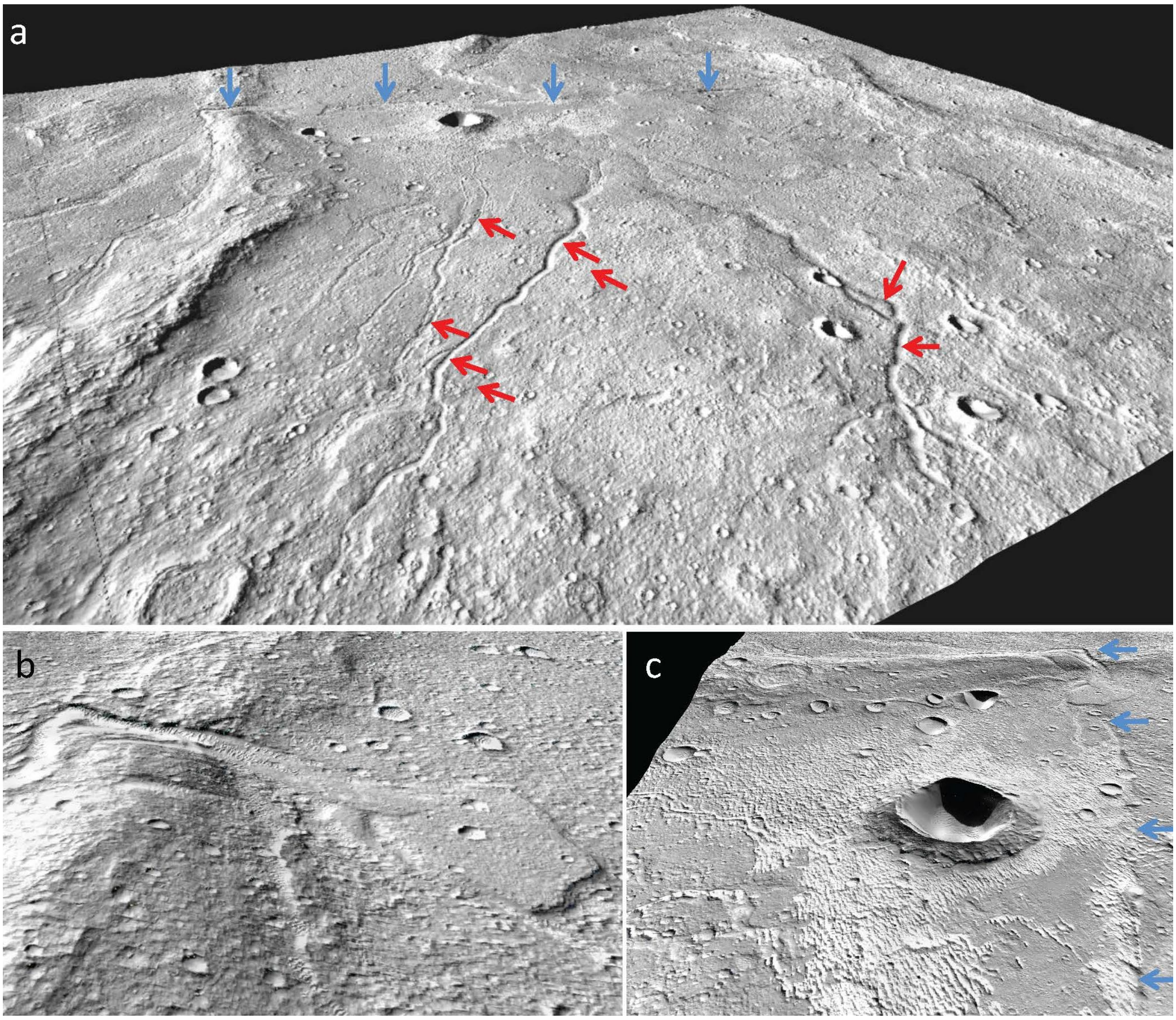

Figure S3. Three-dimensional blocks showing different sedimentary and structural features in the southern sector of the studied area with chloride outcrops. (a) General perspective displaying some sedimentary deposits (blue arrows) and fluvial morphologies (red arrows) that are delimited or constrained by faults. North-oriented channels show both linear and angular features (red arrows) consistent with the structural pattern (see Fig. S1) affecting the eNh and mNh Noachian basement (Tanaka et al., 2014). The channels converge within the salt bodies that are delimited to the north by a fault (blue arrows) with an ESE-WNW strike. (b) Fluvial channel terminating in an alluvial fan that grew towards the SE following the bearing of the ESE-WNW fault shown in panel (a), postdating the salt-filled streams. (c) ESE-WNW bearing fault (blue arrows) which acts as a boundary for the chloride body to the north.

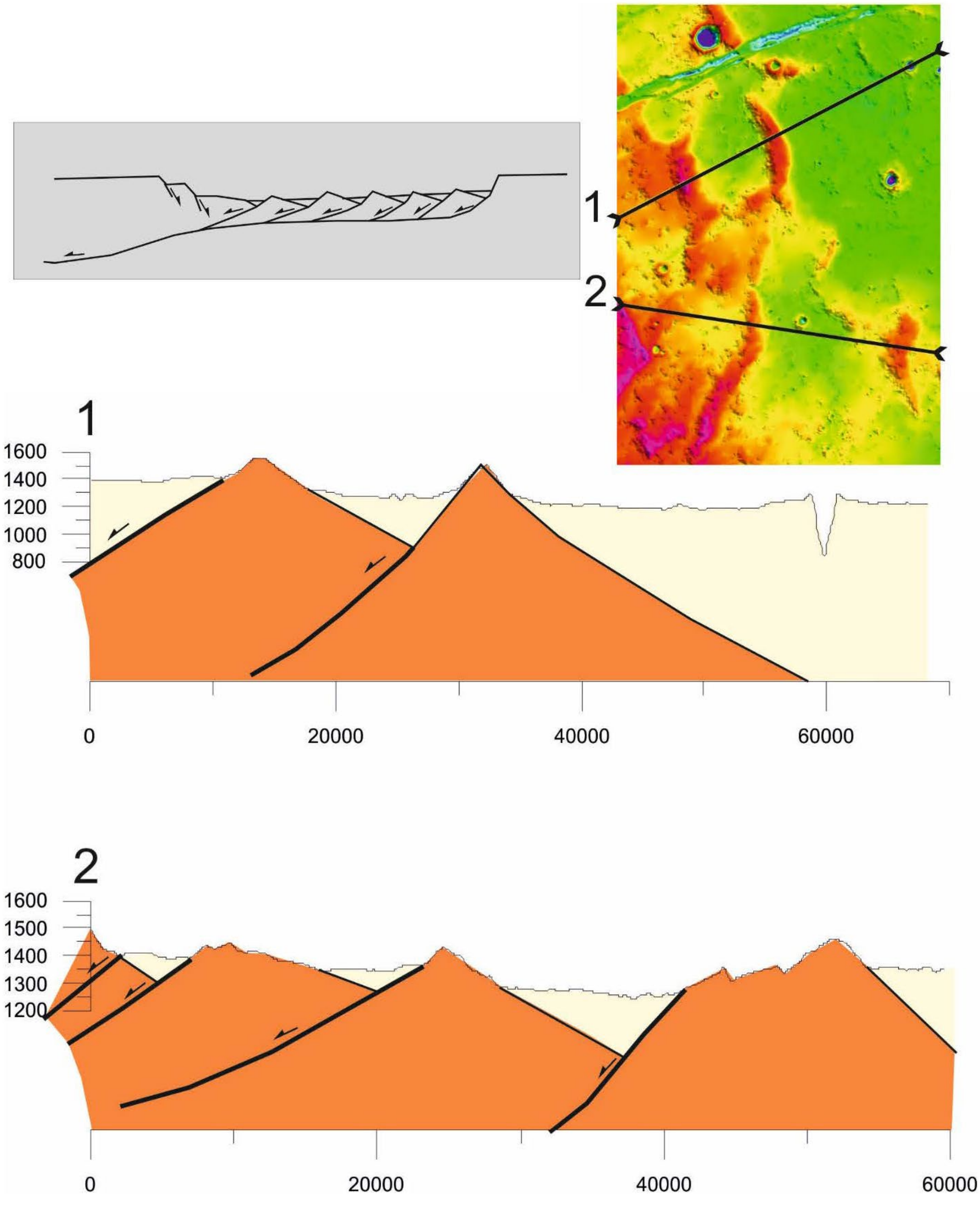

Fig. S4. Tectonic structure suggested for the Terra Sirenum area between Memnonia and the Newton Crater showing chloride deposits. The structure consists of a succession of west-dipping half-grabens that may have transported hydrothermal fluids interacting with the Mars crust. The formation of these half-grabens led to the uplift of the N-S trending ridges that confine different basins within the Noachian terrains of the Mars highlands. Such hydrothermal alteration may have produced acidic solutions in the same way as they are produced in various hydrothermal systems on Earth as described by Seyfried (1987). Vertical and horizontal units are meters.

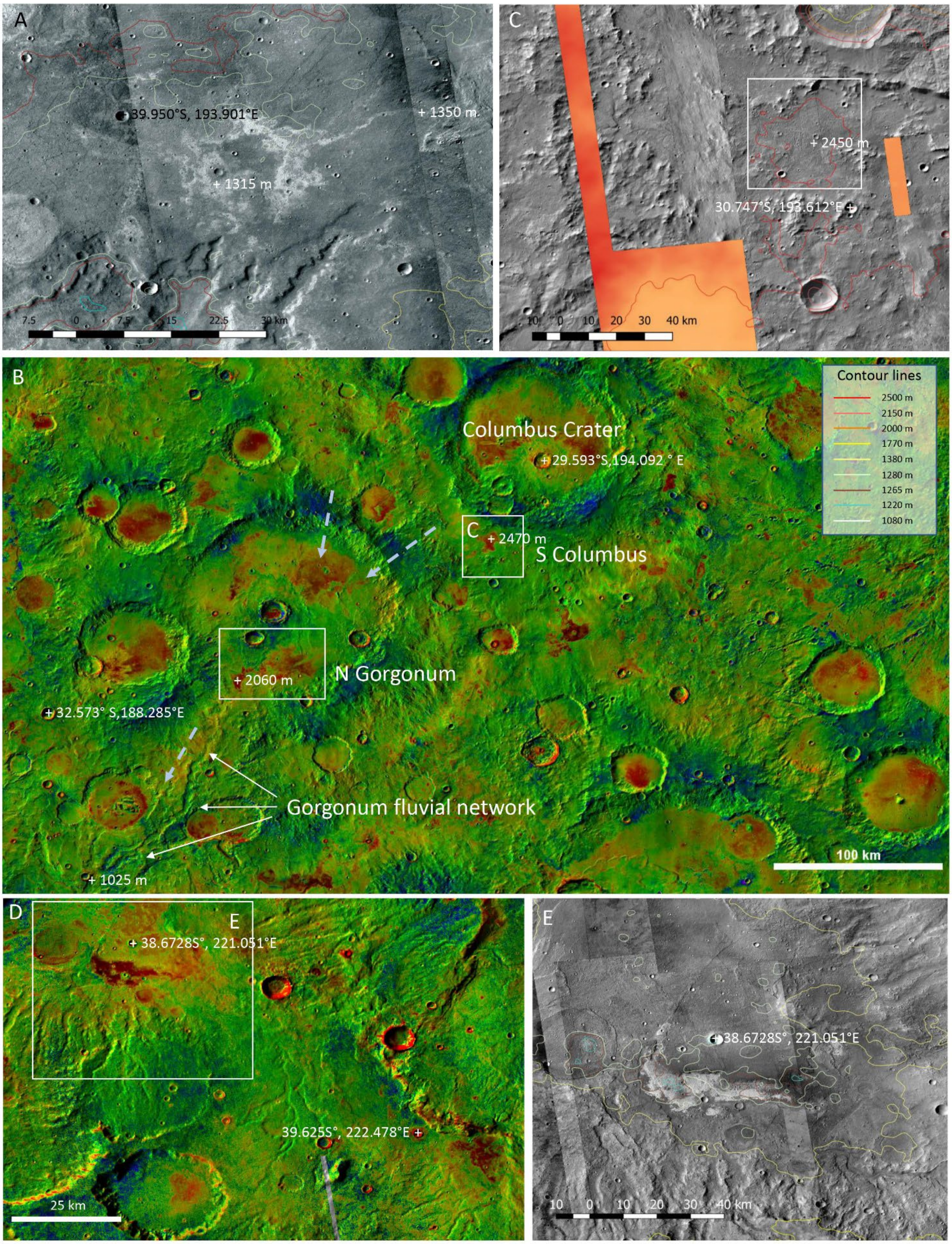

Fig. S5. Different chloride outcrops in Terra Sirenum including E Gorgonum (A), S Columbus (B), N Gorgonum (C), and W Lantang (D and E). Contour lines and averaged altitudes are shown in A, B and D. Images B and D show in some instance however the chloride outcrops in red, which results from a combination of the THEMIS Day IR 100 m Global Mosaic data and the THEMIS Night IR 100 m Global Mosaic following the procedures of Edwards et al. (2011). In S Columbus (C), the white square marks the salt outcrops. The paleohydrological flows are shown as dashed blue arrows. White arrows (A) mark some dikes in E Gorgonum.

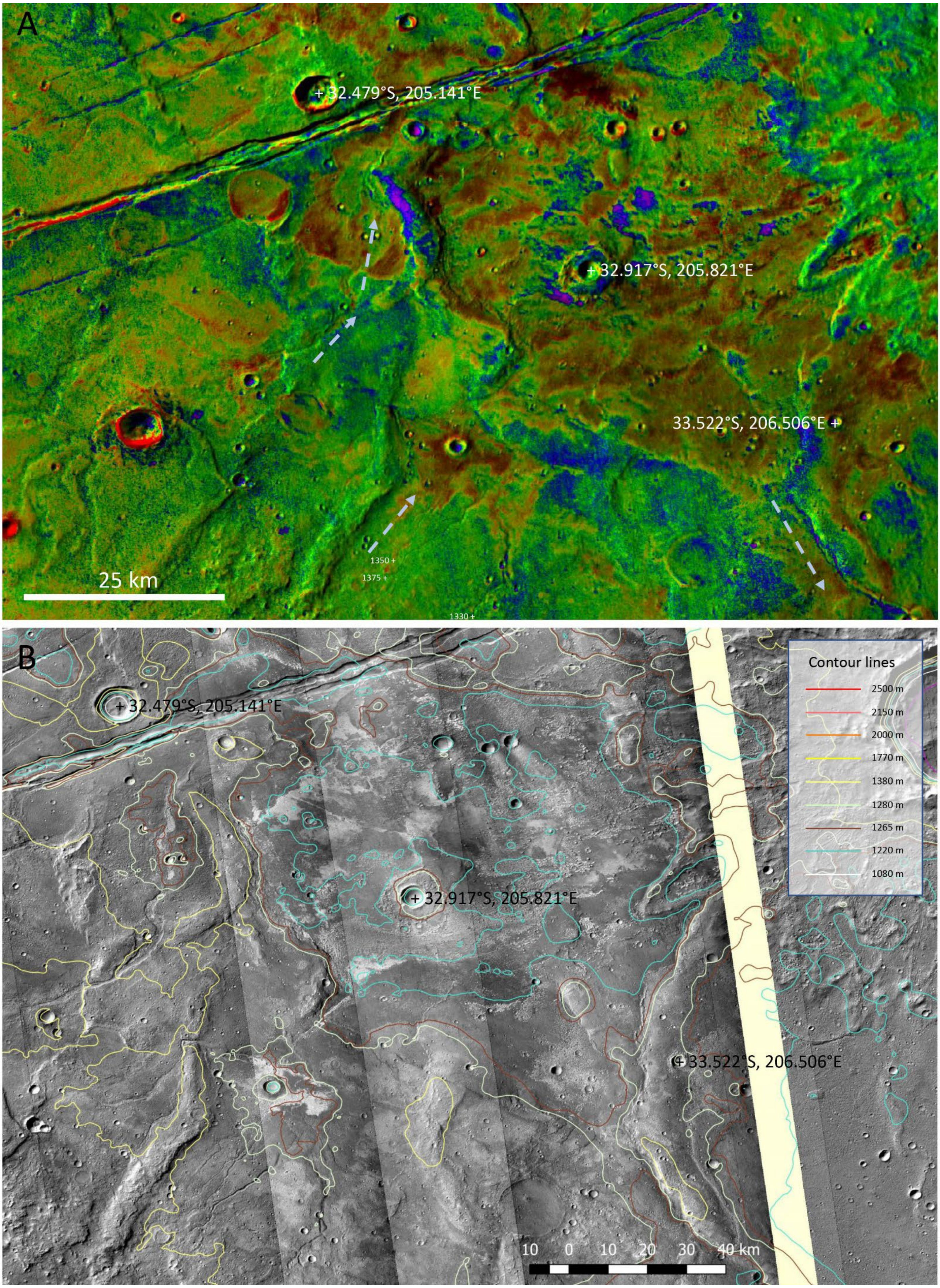
A
+ 32.479°S, 205.141°E
+ 32.917°S, 205.821°E
33.522°S, 206.506°E +
1350 +
1375 +
1330 +
25 km
B
Contour lines
2500 m
2150 m
2000 m
1770 m
1380 m
1280 m
1265 m
1220 m
1080 m
+ 32.479°S, 205.141°E
+ 32.917°S, 205.821°E
+ 33.522°S, 206.506°E
10 0 10 20 30 40 km

Fig. S6. Chloride outcrops in the Sirenum Fossae area shown as red areas (A) that meet the same localities with typical textural and structural features found in the Mars chlorides (B). Different morphological features as: 1) a paleohydrological flow (dashed arrows) heading North, opposite to the fluvial network heading south, 2) an average altitude below 1280 m in association distension structures, and 3) chlorides are associated with channels occurring at a similar altitude of 1380 and 1340 m, suggest a different formation process for chlorides in the Sirenum Fossae location. Image A show the chloride outcrops in red, which results from a combination of the THEMIS Day IR 100 m Global Mosaic data and the THEMIS Night IR 100 m Global Mosaic following the procedures of Edwards et al. (2011).

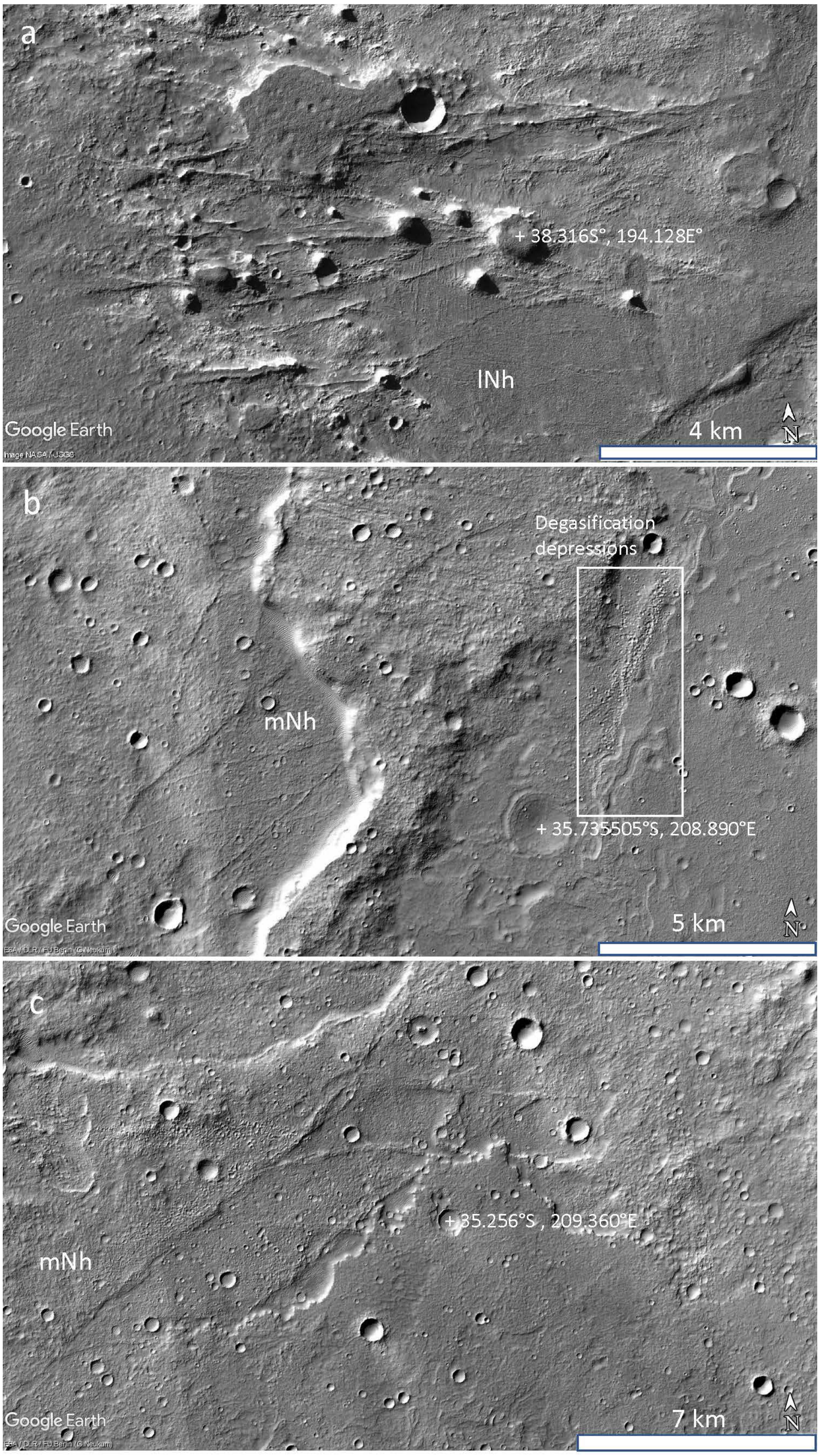

Fig. S7. Images (a) to (c) showing the occurrence of dyke swarms in different locations of Terra Sirenum. In some cases, they can co-occur associated to concentration of ground quasicircular depressions (b) suggesting volatile release by thermal activity. mNh (middle Noachian) and lNh (late Noachian) correspond to the terrain units established by Tanaka et al. (2014), suggesting that dykes are younger than the ancient terrains which are intruding.

a

Anorthite + Fayalite + Forsterite + Diopside + Albite + 21·H_2O + 4.91·Al^{3+} + 3.91·Mg^{2+} + 2·Fe^{2+} → 1.3·Clinoclore-14Å + 2·Chamosite + 0.75·Montmorilonite-Ca + 0.76·Ca^{2+} + Na^{+} + 21.83·H^{+}

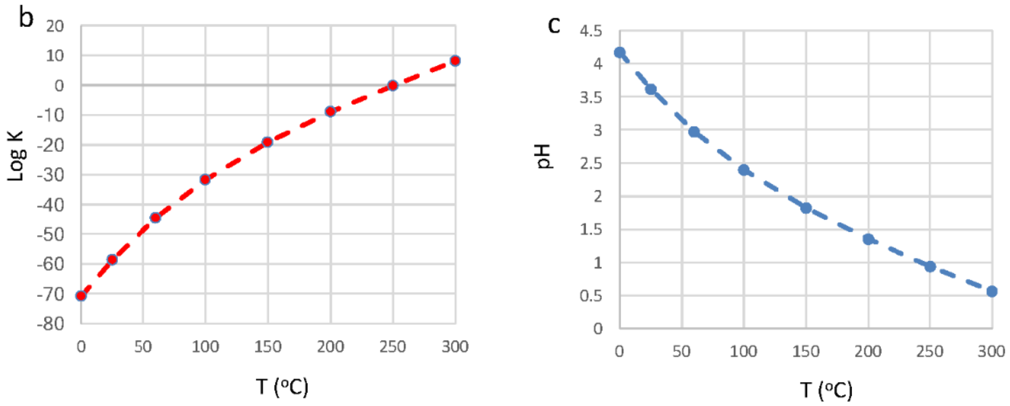

d $\text{Log } K(T) = 0.76 \cdot \log a[Ca^{2+}] + \log a[Na^{+}] - 21.83 \cdot pH - 4.92 \cdot \log a[Al^{3+}] - 3.91 \cdot \log a[Mg^{2+}] - 2 \cdot \log a[Fe^{2+}]$

Anorthite ($CaAl_2Si_2O_8$)
Fayalite (Fe_2SiO_4)
Forsterite (Mg_2SiO_4)
Diopside ($MgCaSi_2O_6$)
Albite ($NaAlSi_3O_8$)
Clinochlore-14Å ($Mg_5Al_2Si_3O_{10}(OH)_8$)
Chamosite ($Fe_2Al_2SiO_5(OH)_4$)
Montmorillonite-Ca ($(Ca)_{0.33}(Al,Mg)_2(Si_4O_{10})(OH)_2 \cdot nH_2O$)
Wustite (FeO)
Magnetite ($Fe^{2+}Fe^{+3}{}_2O_4$)
Quartz (SiO_2)

Fig. S8. Hydrothermal reactions used in this model that promoted the progressive acidification via the alteration of the Martian crust with an increase in the temperature. (a) Main reactions resulting from the combination of the alteration of some common Martian crustal minerals, including olivine (represented by end-members fayalite and forsterite), diopside, plagioclase feldspar (represented by end-members anorthite and albite), some of which produced select phyllosilicates detected on Mars, including chamosite, chlinochlore and montmorillonite. (b) Relationship between the temperature and the reaction constant K, which suggests that the reaction favours an increase in the temperature. Such a relation between K and T results in (c), which produces a decreasing pH when T is increasing. The geochemical calculations that are mathematically expressed in (d) were obtained after substituting the cationic activities and the reaction constant for a given T in the hydrothermal reaction. The cationic activities and reaction constant K were obtained after running a model for the hydrothermal reaction (a) under the REACT module of Geochemist Workbench 12. The input and output of the ionic data obtained after running the model are shown in Table S2.

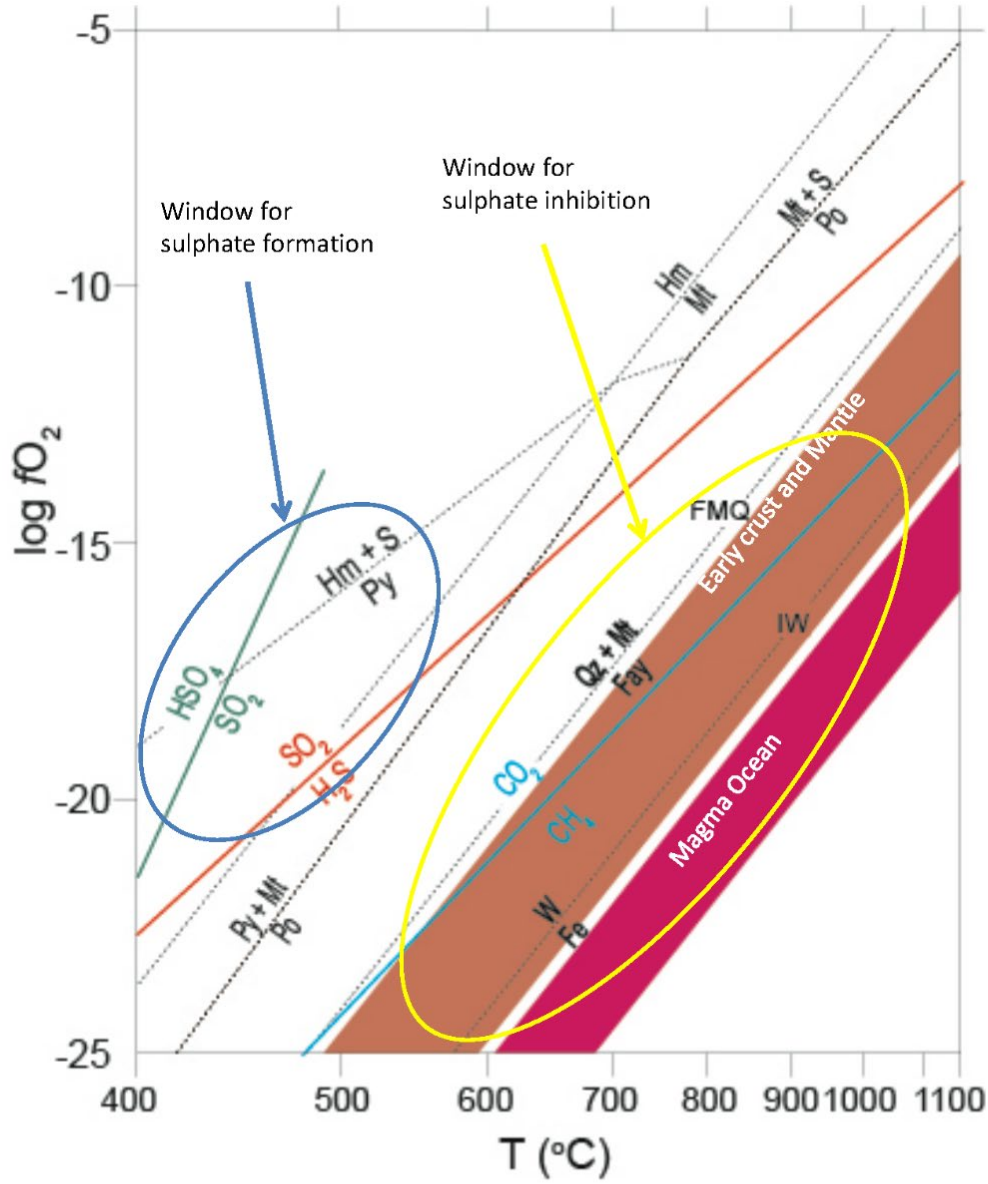

Fig. S9. Oxygen fugacity versus temperature diagram calculated for a pressure of ~ 1 GPa shows the occurrence of different volatiles, such as CO_2, CH_4, SO_2 and H_2S, that are plotted with regard to the FMQ (fayalite-magnetite-quartz) and IW (iron-wüstite) buffer mineral curves (modified after Richards, 2015 with the addition of Mars data from Wadhwa, 2008 and Gaillard et al., 2013). The temperature and pressure of melting/crystallisation, which partially control the oxygen fugacity, played an essential role in the atmospheric chemistry of early Mars. Thermobaric estimates from the oldest Martian meteorites (Richter et al., 2008; Wadhwa, 2008) and from robotic probes operating in situ (Schmidt et al., 2013) suggest that the redox conditions of the Mars interior may have equilibrated to a buffer < FMQ-5 at 4.5 Ga, which may have evolved to an average buffer of FMQ-1. Under these conditions, the volatile inventory is predicted to be dominated by CO_2, CO, H_2S > SO_2, and likely CH_4. Chloride-bearing gases should have been dominated by HCl, which may have occurred at an atmospheric concentration of up to 10-5-10-7 atm assuming that Cl was present in the magmatic sources at concentration >2.5 times higher than known terrestrial igneous reservoirs (Farrand et al., 2007).

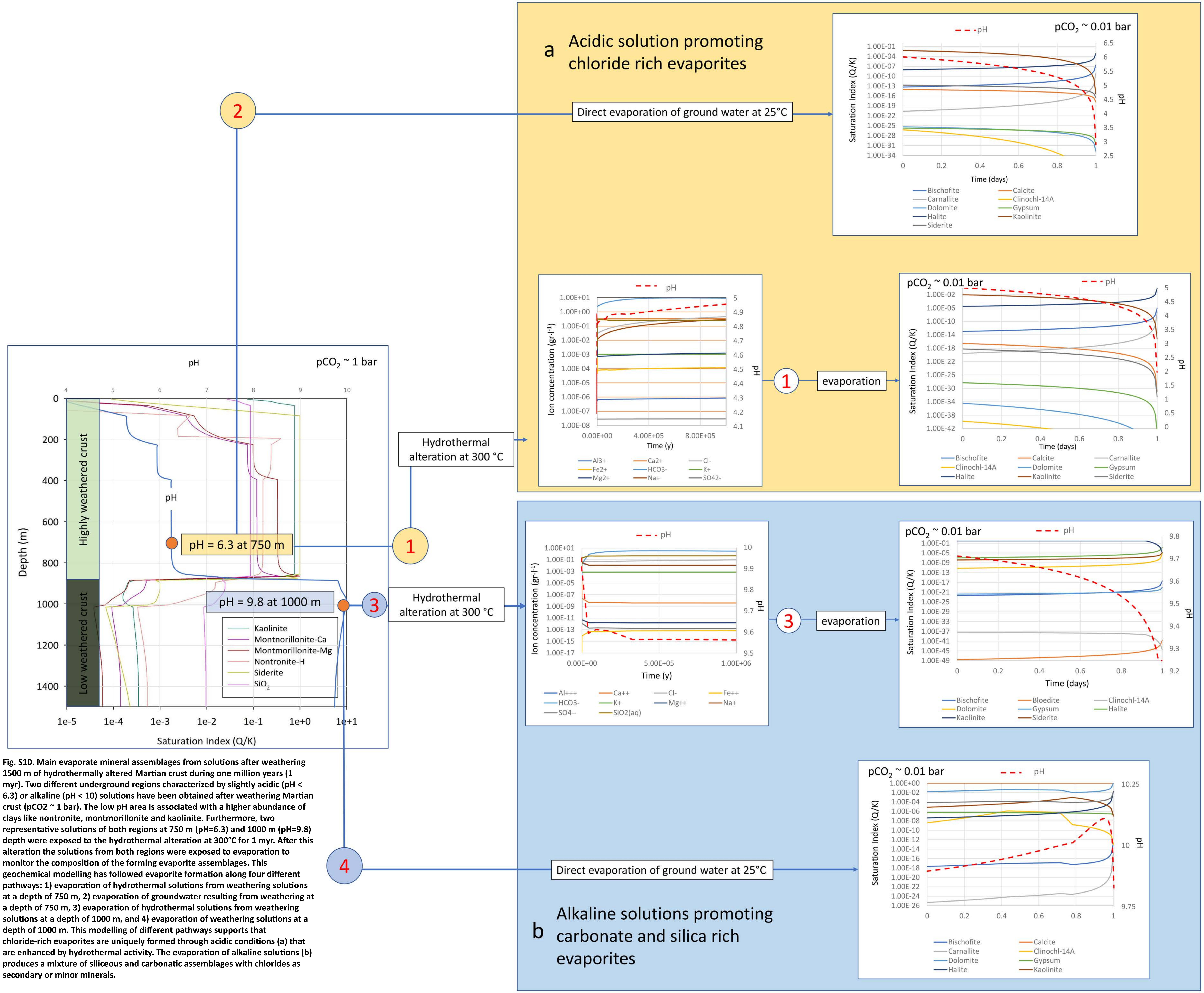

Fig. S10. Main evaporate mineral assemblages from solutions after weathering 1500 m of hydrothermally altered Martian crust during one million years (1 myr). Two different underground regions characterized by slightly acidic (pH < 6.3) or alkaline (pH < 10) solutions have been obtained after weathering Martian crust (pCO2 ~ 1 bar). The low pH area is associated with a higher abundance of clays like nontronite, montmorillonite and kaolinite. Furthermore, two representative solutions of both regions at 750 m (pH=6.3) and 1000 m (pH=9.8) depth were exposed to the hydrothermal alteration at 300°C for 1 myr. After this alteration the solutions from both regions were exposed to evaporation to monitor the composition of the forming evaporite assemblages. This geochemical modelling has followed evaporite formation along four different pathways: 1) evaporation of hydrothermal solutions from weathering solutions at a depth of 750 m, 2) evaporation of groundwater resulting from weathering at a depth of 750 m, 3) evaporation of hydrothermal solutions from weathering solutions at a depth of 1000 m, and 4) evaporation of weathering solutions at a depth of 1000 m. This modelling of different pathways supports that chloride-rich evaporites are uniquely formed through acidic conditions (a) that are enhanced by hydrothermal activity. The evaporation of alkaline solutions (b) produces a mixture of siliceous and carbonatic assemblages with chlorides as secondary or minor minerals.

Table S1. Locations with chloride outcrops in Terra Sirenum shown in Figs 1, and S6-S7.

Area	Coordinate	Elevation (m)	Features
E Gorgonum Chaos	40.028°S, 194.036°E	1325-1290	Deposits associated to a channel outflowing east to 1280 m. The chlorides lay on a flat surface with linear structures that is degraded south with several gullies headed south. Laying on the lNh unit of Tanaka et al. (2014).
Columbus Crater	30.532°S, 193.496°E	2495-2445	Isolated outcrop with no traces of channels occurring outside of the Columbus crater rim. East of the salt deposits is observed a fluvial network heading south. Laying on the eNh unit of Tanaka et al. (2014).
N Gorgonum Chaos	32.050°S, 191.020°E	2090-2045	Upstream of a large channel flowing to Gorgonum chaos, which start inside of a highly degraded crater. Laying on the lNh unit of Tanaka et al. (2014).
Sirenum Fosae (three sedimentary bodies limited by NW-SE faults)	33.342°S, 205.565°E 32.892°S, 205.757°E 32.631°S, 205.738°E	1290-1265 1240-1210 1230-1205	Complex and large chloride outcrops limited by faults and connected to channels with positive relief filled with chlorides as well. Channels occur at an average altitude of ~ 1350 m. Laying on the mNh unit of Tanaka et al. (2014).
NE Sirenum Tholus	33.495°S, 216.225°E 33.313°S, 216.300°E	1400-1355	Partially covered deposits apparently cropping out in a bed of a long channel flowing northwards. The channel could be part of a watershed recharged by the volcanic dome of Sirenum Tholus at around 2000 m of altitude. Laying on the mNh unit of Tanaka et al. (2014).
SE Sirenum Mons	39.431°S, 216.485°E 39.768°S, 216.337°E	1990-1935	Chloride deposits associated to a channel network occurring at ~ 2100 m inflowing northwards where the chlorides occur. Laying on the eNh unit of Tanaka et al. (2014).
W Lantang Crater	39.625S°, 222.478°E 38.815S°, 221.045°E	1895-1875 1310-1270	Two different outcrops occurring at an average altitude of 1860 and 1270 m respectively. They are associated to well-developed fluvial network inflowing convergently to the salt deposits. The lower outcrop is outlined by the 1280-m contour. line that suggests a lacustrine origin. The sedimentary settings in both outcrops are consistent with playa-lake or sabkha systems. Laying on the mNh unit of Tanaka et al. (2014).

Table S2. Mineral composition used for the geochemical modelling for the chloride-forming deposits in Terra Sirenum after weathering, hydrothermal alteration and precipitation shown in Figs. 4, and S10.

Mineral composition of Mars crust (wt %)		
Mineral	**Composition**	**wt %**
Anorthite	$CaAl_2Si_2O_8$	19.0
Albite	$NaAlSi_3O_8$	17.0
Diopside	$MgCaSi_2O_6$	13.2
Fayalite	Fe_2SiO_4	24.6
Forsterite	Mg_2SiO_4	26.2

Table S3. Composited table for Geochemical and mineral data used for modelling the weathering of the Martian crust at 25°C following by its alteration by hydrothermalism at 300 °C. The modelling was initiated by a subsaturated solution replicating rainwater in equilibrium with a CO_2-rich atmosphere (1 bar) including other volatiles as H_2S (10^{-5} atm) and HCl (10^{-7} atm) (Gaillard et al., 2013; Ramirez and Cradock, 2018). The hydrochemistry table is showing the resulting composition of the solutions after the 1 Ma weathering of a 1.5 km basaltic crust followed by an additional 1-Ma episode of hydrothermal alteration. The most outstanding result is the strong decreasing of pH under hydrothermal alteration of the Mars crust, which prevents the carbonate precipitation in a first stage. The resulting pH from the hydrothermal episode is changed to 4.9 and 5.5 and 9.6 when the initial pH resulting from weathering varies between 6.3 (750 m depth) and 9.9 (1500 m depth), respectively (see Fig. 4). Weathering was induced under a water flow of $2\cdot10^{-1}$ m·yr^{-1} (boundary between semiarid and arid climates). The precipitation of carbonates is definitively inhibited when the solutions of 4.9 pH solutions of hydrothermal origin are evaporated to produce uniquely chlorides, while the 9.6 pH hydrothermal solutions sourced an evaporitic paragenesis dominated by carbonates and silicates.

Geochemical parameters	**Weathering of Mars crust (T = 25°C)**		**Hydrothermal alteration (T = 300°C)**	
T (°C)	25		300	
Eh (V)	-0.25		-0.25	
Depth (m)	750	1000	750	1000
pH	4 to 6.3	4 to 9.9	6.3 to 4.9	9.9 to 9.6/5.5*
SiO_2	1.10E-02	3.90E-03	2.55E-01	4.84E-01/1.58E-01
Fe^{2+}	1.88E-03	2.29E-08	1.18E-04	1.50E-13/7.80E-04
Mg^{2+}	2.48E-01	1.58E-06	1.25E-03	2.46E-12/5.75E-03
Ca^{2+}	4.37E-03	2.75E-03	3.33E-01	3.93E-09/2.36E+00
Na^+	1.01E-02	3.42E-02	2.94E-01	1.22E-02/3.19E-01
K^+	1.01E-03	7.10E-04	1.04E-03	7.33E-04/7.35E-04
Al^{3+}	4.31E-08	8.23E-08	8.25E-07	1.05E-02/7.86E-18
Cl^-	2.09E-02	4.46E-02	4.67E-01	4.78E-01/4.84E-01
HCO_3^-	2.46E+00	2.68E-02	9.28E+00	3.15E+00/3.20E+00
SO_4^{2-}			2.90E-08	1.95E-13/4.61E-18

*Alkaline weathering solutions could evolve to acidic through hydrothermal alteration if an additional meteoric inflow of $2\cdot10^{-1}$ m·yr^{-1} is provided, which would produce a flux of Mg ~ 10^{-18} mol·yr^{-1}. This suggests that the climatically controlled hydrological activity promotes the acidification under hydrothermal activity.

Table S4. List of CTX images showing chlorides in Terra Sirenum.

F04_037286_1469_XI_33S155W,	D22_035796_1467_XI_33S155W,
P17_007736_1455_XN_34S155W,	P18_008171_1473_XN_32S154W,
F01_036218_1468_XI_33S155W,	B11_014065_1463_XI_33S154W,
F02_036429_1469_XI_33S154W,	B08_012741_1750_XN_05S010W,
P05_003160_1413_XI_38S139W,	F04_037181_1397_XN_40S166W,
B20_017428_1499_XN_30S166W,	B05_011547_1468_XN_33S168W,
F01_036113_1472_XN_32S169W,	B03_010900_1398_XN_40S143W,
B08_012601_1399_XN_40S143W,	P15_007050_1462_XI_33S143W

References

Farrand, W. H., Bell, J. F., Johnson, J. R., Jolliff, B. L., Knoll, A. H., McLennan, S. M., Squyres, S. W., Calvin, W. M., Grotzinger, J. P., Morris, R. V., Soderblom, J., Thompson, S. D., Watters, W. A., Yen, A. S. Visible and near-infrared multispectral analysis of rocks at Meridiani Planum, Mars, by the Mars Exploration Rover Opportunity. *Journal of Geophysical Research* **112**(E6), 10.1029/2006JE002773 (2007).

Gaillard, F., Michalski, J., Berger, G., McLennan, S. M., Scaillet, B. Geochemical Reservoirs and Timing of Sulfur Cycling on Mars. *Space Science Reviews* **174**, 251-300 (2013).

Seyfried W. E. Experimental and Theoretical Constraints on Hydrothermal Alteration Processes at Mid-Ocean Ridges. *Annual Review of Earth and Planetary Sciences* **15**,317-335 (1987).

Richards, J. P. The oxidation state, and sulfur and Cu contents of arc magmas: implications for metallogeny. *Lithos* **233**, 27-45, doi:http://dx.doi.org/10.1016/j.lithos.2014.12.011 (2015).

Richter, K., Yang, H., Costin, G. & Downs, R. T. Oxygen fugacity in the Martian mantle controlled by carbon: New constraints from the nakhlite MIL 03346. *Meteoritics & Planetary Science* **43**, 1709-1723 (2008).

Schmidt, M. E., Schrader, C. M., McCoy, T. J. The primary fO_2 of basalts examined by the Spirit rover in Gusev Crater, Mars: Evidence for multiple redox states in the martian interior. *Earth and Planetary Science Letters* **384**, 198-208, doi:http://dx.doi.org/10.1016/j.epsl.2013.10.005 (2013).

Tanaka K., Skinner, J. A., Dohm, J. M., Rossman, P. I., Kolb, E. J., Fortezzo, C. M., Platz, T., Michael, G. G., Hare, T. M. Geological Map of Mars, cale 1:20,000,000. in U.S. Geological Survey Scientific Investigations (US Geological Survey, Arizona) (2014).

Wadhwa, M. Redox conditions on small bodies, the Moon and Mars. *Reviews in Mineralogy & Geochemistry* **68**, 493-510 (2008).